Hybrid model simulation of a plasma plume in a magnetic nozzle

IEPC-2011-048

Presented at the 32nd International Electric Propulsion Conference,
Wiesbaden, Germany
September 11–15, 2011

Jaume Navarro* and Eduardo Ahedo†
E.T.S. Ingenieros Aeronáuticos, Plaza Cardenal Cisneros, Madrid 28040, Spain

The following research inquiries into the plasma expansion in a divergent magnetic nozzle using an axilsymmetric hybrid code. This code is derived from a previous one for Hall-effect thrusters. It is based on Particle-in-cell (PIC) methods for ions and neutrals, and anisotropic fluid model for electrons, assuming they are strongly magnetized. The PIC subcode provides a map of densities and fluxes of heavy species. Likewise, the code assumes the plasma to be quasineutral. Ion streamtubes are found to detach from electron/magnetic streamtubes, thus agreeing with results from a fluid code of our own. The behavior of the magnetic nozzle on the plasma plume expansion is contrasted with simulations of an unmagnetized plasma plume.

I. Introduction

Some propulsion devices propose the divergent magnetic nozzle as an efficient mechanism to accelerate the plasma, generated upstream, inside the thruster discharge chamber, like the Helicon thruster,[1–4] the applied-field magnetoplasmadynamic thruster,[5] and the VASIMR.[6] Merino and Ahedo[7–11] have carried out studies of supersonic plasma expansion along the divergent magnetic nozzle. Most of the results have been obtained with DIMAGNO, the numerical code associated to a two-dimensional fluid plasma/nozzle model. They analyzed the plasma radial and axial expansion, the plasma currents and the main magnetic nozzles performances in terms of thrust gain and thrust efficiency.

The present investigation tries to make inquiries on the resourcefulness of an axilsymmetric hybrid code to simulate the plasma expansion inside a divergent magnetic nozzle. The hybrid model physical and mathematical bases were summarized by Parra et al.,[12] and it solves the most important aspects of Hall-effect thrusters performances. Some modifications have been introduced since 2005 in order to simulate other physical processes, such as the improvement of the plasma-wall interaction models,[13,14] the Bohm condition fulfillment in the transition between the quasineutral domain and the non-neutral plasma sheath near the wall,[15] and other improvements related to numerical algorithms.

The former hybrid code has been reorganized to figure out the new topology of the present problem, the divergent magnetic nozzle. Required changes affect both the electron fluid subcode and the PIC algorithms. Besides, the new version is able to simulate the expansion of an unmagnetized plasma, neglecting the effects of the magnetic nozzle. Subsequently, it provides the opportunity to draw a comparison between each acceleration mechanism.

In the current step of development, electrons will be take for granted to be isothermal. However, a previous analysis of the problem gives us enough information to consider the non-isothermal case. At the moment, it is being built up, but it might require substantial modifications on the numerical scheme on the former electron fluid subcode due to numerical instabilities.

This study also confirms that current ambipolarity is not fulfilled everywhere inside the plasma expansion in a divergent magnetic nozzle topology. The fulfillment of this conjecture presents some incompatibilities with basic laws such as charge conservation.[16]

*PhD student, jaume.navarro@upm.es
†Professor, eduardo.ahedo@upm.es (web.fmetsia.upm.es/ep2)

This article is structured in the following way. In a fist place, we will summarize the former hybrid code important modifications. In a second place, the key points of the plasma model expansion in a divergent magnetic nozzle will be derived. In a third place, a plasma expansion simulation through a divergent magnetic nozzle will be compared with the plasma expansion without magnetic nozzle effects. Finally, a summary of the main conclusions and future improvements will be announced.

II. Modifications on the former hybrid code

In order to clarify the most important variations, a brief discussion about the original hybrid code is necessary to understand all introduced changes. The code can be divided into two very different parts: the PIC subcode, and the electron subcode. The first one provides the plasma density n_e distribution and ion current densities $\boldsymbol{j}_i$ to the second one. Consequently, the electron subcode returns the electron temperature T_e, the electric potential ϕ, and the perpendicular electric current $I_\perp$ through each magnetic surface. The three last plasma variables are one-dimensional, constant along each magnetic surface and inputs for the PIC subcode.

It is also necessary to emphasize that each subcode uses different meshes to do computations on it (Fig. 1). The electron subcode mesh is derived from the magnetic field. This field is stationary. A low-beta plasma is considered, so that the induced magnetic field, due to plasma currents, can be neglected when compared with the applied field. The field particularities allow us to get the magnetic streamfunction. Each magnetic line (or magnetic surface, if axilsymmetry is assumed) constitutes a node for the electron subcode, and all fluid dynamics equations will be projected on them. In addition, referring to the PIC subcode, we could distinguish two meshes: the $r-z$ mesh and the computational grid. The first one is a cylindrical prism lengthwise section where particles are moved according to electromagnetic and inertial forces. Also, the computational grid is a rectangular auxiliary mesh, which is necessary for weighting PIC algorithms. Both electrons, as well as the PIC meshes, were prepared to deal with a very restrictive topology of conventional Hall thrusters, such as the SPT-100. The greatest effort carried out in this project, in terms of software development, has consisted on making it more flexible and adapting all subroutines to the new proposal.

The most important modifications are listed below.

1. **Boundary conditions** were intrinsically implemented in the former hybrid code. To give an example, observing the computational grid, all the escaped ions from the computational domain through the bottom or top boundaries were recombined automatically because the code assumed these boundaries to be walls. New conditions are extremely different now. The $r-z$ and its linked computational grid will assume right and top boundary to be vacuum, bottom boundary to be the axis of symmetry and left boundary to be, either wall or plasma injector (magnetic nozzle throat).

2. **Axis of symmetry** is included into the domain. It is the bottom boundary of the PIC mesh. Reducing the miscalculation tolerance between each particle position in the $r-z$ plane and its position in the computational grid is a required change to avoid inconsistencies of numerical weighting algorithms.

3. **Particle injection subroutine** requires significant modifications. The new version makes possible to introduce the density profile of the plasma along the panels that make up the injection section. This section can be located along a chosen range of panels in the left boundary.

4. **Electron mesh**, defined by the magnetic topology, was simple for a common Hall thruster. Every line intercepts both, bottom and top PIC boundaries, always finding wall conditions at the end of each line, wich make the process of stream function discretization to be easier, but some difficulties in the anode region (left boundary of PIC subcode) appeared. Magnetic lines can indistinctly intercept all PIC boundaries now. The last magnetic line coincides with the axis of symmetry. The new topology requires redefining all the boundary conditions at the end of each magnetic stream line depending on the PIC boundary that is intercepted.

5. **The electron temperature solver**, based on the solution of the electron energy equation is provisionally blocked because T_e is assumed constant.

6. **Ionization subroutines** are also blocked to simplify the plasma model. Furthermore, we will only take into account simple ions.

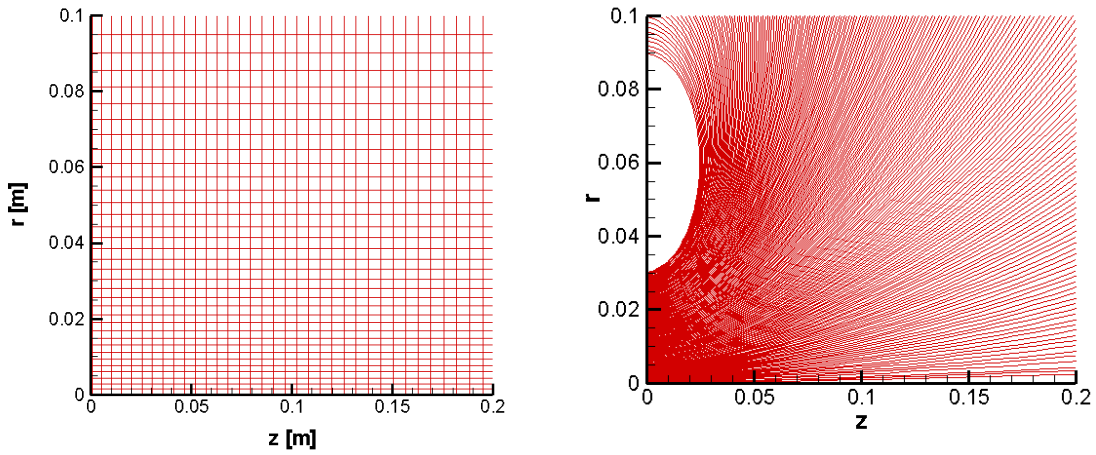

Figure 1. PIC $r-z$ mesh (left) and magnetic mesh (right)

III. Plasma model in a magnetic nozzle

First of all, we summarize the process to obtain the magnetic mesh from the magnetic field topology. This field, created by a coil system, is solved during the pre-process using a commercial FEM code. The zero-vorticity and zero-divergence of the magnetic field, $\nabla \times \boldsymbol{B}$ and $\nabla \cdot \boldsymbol{B}$ respectively, let us to assure the magnetic stream function λ exists and satisfies,

$$\frac{\partial \lambda}{\partial z} = -rB_r \qquad \frac{\partial \lambda}{\partial r} = rB_z \tag{1}$$

where B_z and B_r are the magnetic field components expressed on a cylindrical reference frame $\{\mathbf{1}_z, \mathbf{1}_r, \mathbf{1}_\theta\}$. The magnetic reference frame will be $\{\mathbf{1}_\perp, \mathbf{1}_\parallel, \mathbf{1}_\theta\}$ in which $\mathbf{1}_\parallel = \boldsymbol{B}/B = \cos\alpha \mathbf{1}_z + \sin\alpha \mathbf{1}_r$, $\mathbf{1}_\perp = \sin\alpha \mathbf{1}_z - \cos\alpha \mathbf{1}_r$ and $\alpha(r,z)$ is the local magnetic angle. Each different λ value, belongs to a different magnetic streamline, in which λ, T_e, $I_\perp$, and the thermalized potential ϕ_0 (defined below) are constant. Differential control volumes are defined for each streamline. The streamline revolution around the axis of symmetry, defines a magnetic surface.

Further, we will submit the electron fluid dynamics equations, basically, mass conservation and momentum equation. In this case, energy equation is omitted because T_e is constant.

$$\frac{\partial n_e}{\partial t} + \nabla \cdot (n_e \boldsymbol{u}_e) = \dot{n}_e \tag{2}$$

$$n_e m_e \left(\frac{\partial \boldsymbol{u}_e}{\partial t} + \boldsymbol{u}_e \cdot \nabla \boldsymbol{u}_e \right) = -\nabla p_e - e n_e (\boldsymbol{E} + \boldsymbol{u}_e \times \boldsymbol{B}) + \boldsymbol{M} \tag{3}$$

Equation 2 can be combined with the ion continuity equation, which has the same form. Afterwards, assuming the hypothesis of quasineutral plasma ($n_e \approx n_i$) and the lack of ionization processes, it yields the charge conservation law,

$$\nabla \cdot \boldsymbol{j} = 0, \tag{4}$$

where $\boldsymbol{j}$ is the electric current density.

Analyzing the electron momentum equation, some assumptions should be taken. $\boldsymbol{M}$ include all collisional effects and it can be written $\boldsymbol{M} = -n_e m_e \nu_e \boldsymbol{u}_e$, where ν_e is the effectively electron collision frequency and takes into account *electron-ion* and *electron-neutral* collisions. This frequency can also include other plasma physical processes related to the plasma wall interaction, virtual cathode considerations and anomalous diffusion. In this work, anomalous diffusion and virtual cathode contribution are not taken into account. The inertial term can be neglected due to the significant difference between electron mass, and ion mass $m_e/m_i \ll 1$. Moreover, this convective term is lower than the electromagnetic force, on the right side of the equation,

$$\|n_e m_e \boldsymbol{u}_e \cdot \nabla \boldsymbol{u}_e\| / \|e n_e \boldsymbol{u} \times \boldsymbol{B}\| \sim r_L u_e / R v_{te} \ll 1.$$

Here, r_L is the Larmor electron gyroradius, R the magnetic nozzle throat radius and v_{te} the electron thermal velocity. Electron pressure p_e can be written as a function of its temperature $p_e = n_e T_e$, and the electric field $\boldsymbol{E}$ derives from a scalar potential $\boldsymbol{E} = -\nabla\phi$. This last assumption comes from both $\nabla \times \boldsymbol{E} = 0$ and $\nabla \cdot \boldsymbol{E} = 0$ because *(i)* we neglect $\boldsymbol{B}$ field fluctuations in time and *(ii)* assume that plasma is quasineutral. After all these assumptions, momentum equation is reduced to

$$\mathbf{0} = -T_e \nabla n_e + e n_e \nabla\phi - e n_e \boldsymbol{u}_e \times \boldsymbol{B} - n_e m_e \nu_e \boldsymbol{u}_e \tag{5}$$

Electron momentum equation can be projected according $\mathbf{1}_\parallel$ direction obtaining,

$$0 = -T_e \frac{\partial n_e}{\partial \mathbf{1}_\parallel} + e n_e \frac{\partial \phi}{\partial \mathbf{1}_\parallel} \tag{6}$$

Note the collisional term in the Eq. 6 has been scorned in collating with the expected pressure gradients,

$$\frac{\| n_e m_e \nu_e \boldsymbol{u}_{e\parallel} / B \|}{\| T_e \partial n_e / \partial \mathbf{1}_\parallel \|} \sim \frac{u_{e\parallel} R}{v_{te} \lambda_{col}} \ll 1$$

In the last expression, λ_{col} is the electron collision mean-free-path and we characterize these orderings inside the plasma: $\lambda_D \ll r_L \ll R \ll \lambda_{col}$; λ_D is the Debye length. Equation 6 can be integrated, yielding the Boltzmann relation

$$\phi(r,z) = \phi_0(\lambda) + \frac{T_e(\lambda)}{e} \ln\left(\frac{n_e(r,z)}{n_{ref}}\right); \tag{7}$$

$\phi_0(\lambda)$ is the thermalized potential and n_{ref} is any reference density. The Boltzmann relation determines the electric potential in terms of one-dimensional variables (T_e and ϕ_0) and the plasma density distribution determined by the PIC subcode.

Now, we project momentum equation on $\mathbf{1}_\perp$ and $\mathbf{1}_\theta$ respectively,

$$- T_e \frac{\partial n_e}{\partial \vec{1}_\perp} + e n_e \frac{\partial \phi}{\partial \vec{1}_\perp} + e n_e u_{e\theta} B - \nu_e m_e n_e u_{e\perp} = 0 \tag{8}$$

$$- e n_e u_{e\perp} B - \nu_e m_e n_e u_{e\theta} = 0 \tag{9}$$

After some algebraic manipulation, these two equations allow us to obtain expressions for $\boldsymbol{u}_{e\perp}$ and $\boldsymbol{u}_{e\theta}$,

$$u_{e\theta} = -\beta_e u_{e\perp}, \tag{10}$$

$$u_{e\perp} = \frac{r}{\beta_e} \frac{\partial \phi_0(\lambda)}{\partial \lambda}; \tag{11}$$

$\beta_e = \Omega_{ce}/\nu_e$ is the Hall parameter, and Ω_{ce}, is the electron gyrofrequency. We assume again constant temperature and moreover $\beta_e \gg 1$. Note that equation 11 is the Ohm´s law here.

A. Plasma conditions in the magnetic nozzle throat

In a Hall effect thruster, we usually consider that mass injection section coincides with the anodic wall of this device. Likewise, only neutral particles are injected through this boundary. Conditions are extremely different now. First of all, a free-current and fully-ionized plasma jet is injected at the magnetic nozzle throat. And the key point is the equilibrium between magnetic pressure, which confines the plasma, and plasma pressure, which tries to expand it,

$$0 = -T_e \partial_r n_e - e n_e u_{e\theta} B_\parallel. \tag{12}$$

The balance between these forces is achieved thanks to the plasma behavior upstream the nozzle, in the plasma source. In conclusion, the radial electric field must be zero along the magnetic nozzle throat. This condition combined with the Boltzmann relation yields an important constrain for the thermalized potential along all magnetic streamlines that goes through the throat section,

$$\phi_0 = -\frac{T_e}{e} \ln \frac{n_e}{n_{ref}}\bigg|_{z=0}. \tag{13}$$

Therefore, $\phi_0(\lambda)$ is defined by the radial distribution of the plasma density at the throat. For the simulations here, this plasma distribution is assumed to be parabolic, $n_e(r) = A(1-(r/R)^2)+B$. A and B are numerical constants and depend on some parameters such as the desired mass flow, the averaged ion speed at the throat and the ion density background. Ion velocity will be sonic at the throat, taking ion sound speed defined as $c_s = \sqrt{T_e/m_i}$, where m_i is the simple ion mass.

As a consequence of all concepts explained before, the determination of ϕ_0 and $I_\perp$ must be divided into two parts, depending on the region of the magnetic mesh that we consider. The first zone is defined by all magnetic streamlines that intercept the magnetic nozzle throat, whereas the second one is composed by the rest of streamlines. In this research, we have realized that is necessary to use different methodologies to solve each region due to the variability of the physical constrains.

B. Solving the internal region

As it has been announced, in the internal region, $\phi_0(\lambda)$ is determined by equation 13. As a result, $I_\perp(\lambda)$ must be obtained assuring the fulfillment of the charge conservation law (Eq. 4) in each magnetic differential volume. This restriction implies that current ambipolarity condition has not been assumed everywhere. To note this result, we will project Eq. 4 on the magnetic mesh, and after some algebraic operations it commutes to

$$\frac{\partial I_\perp(\lambda)}{\partial \lambda} = -\left.\frac{2\pi j}{(B\cos\alpha)}\right|_0 - \left.\frac{2\pi j}{(B\cos\alpha)}\right|_1 \tag{14}$$

This shows how the variation on the perpendicular current through each magnetic surface is caused by the loss or gain of net charge current at the domain boundaries. Subscript 0 and 1 refers to plasma properties just at the magnetic streamlines boundaries, being 0 the boundary located closest to the left bottom corner of the PIC domain (magnetic throat). Current densities j are positive according to the orthogonal outward vector for the PIC domain boundary. α is the angle between the mentioned vector and the local vector $\mathbf{1}_\perp$.

In all expressions $I_\perp(\lambda)$ is defined as the integral of the density current along the magnetic surface. Naturally, it needs to be contributed by both, the perpendicular current of ions and electrons.

$$I_\perp(\lambda) = \iint_{S(\lambda)} (\boldsymbol{j}\cdot\boldsymbol{u}_\perp)dS = \iint_{S(\lambda)} (\boldsymbol{j}_i\cdot\boldsymbol{u}_{i\perp}) + (\boldsymbol{j}_e\cdot\boldsymbol{u}_{e\perp})dS = \int_{\Gamma(\lambda)} 2\pi r e n_e(\boldsymbol{u}_i - \boldsymbol{u}_e)\cdot\boldsymbol{u}_\perp d\chi = I_{i\perp}(\lambda) + I_{e\perp}(\lambda) \tag{15}$$

Here the ion contribution $I_{i\perp}(\lambda)$ is obtained by the PIC subcode, whereas $I_{e\perp}(\lambda)$ depends on the reduced Ohm law (Eq. 11) resulting in

$$I_{e\perp}(\lambda) = -\int \frac{2\pi e n_e r^2}{\beta_e} d\chi \left(\frac{\partial \phi_0}{\partial \lambda}\right). \tag{16}$$

As a consequence, $\partial_\lambda I_\perp(\lambda) \neq 0$. Concerning the current ambipolarity condition, it can be imposed only at one of the two ends. In this study, it is forced at the throat and, from the charge conservation, the current density downstream, $\boldsymbol{j}|_1$, fulfills

$$j|_1 = -\frac{\partial I_\perp(\lambda)}{\partial \lambda}\frac{B\cos\alpha}{2\pi}. \tag{17}$$

On the other hand, note that the free-current plasma condition must be globally accomplished. This constrain provides an expression to control the committed error in the internal region,

$$\epsilon_c = -I_\perp(\lambda_V) + \int_{axis}^{\lambda_V} (\boldsymbol{j}(\lambda)\,\boldsymbol{dS}(\lambda))\,|_1 \simeq 0; \tag{18}$$

λ_V is the upper magnetic borderline of the plasma beam at the throat. In the simulations below, the error (ϵ_c) in the free-current constrain is lower than 1% in comparison to the equivalent ion current injected at the throat, $e\dot{m}_i/m_i$.

C. On the transitional boundary and the external region

When this project was started, we expected a gentle enough transition of plasma properties at the nominal plasma jet edge, between the internal region and the near-vacuum region. But our preliminary results

show this transition not to be as gradual as we expected. The essential problem remains on the charge conservation law fulfillment on the outside region, and the lack yet of convincing models to estimate the current density at the top vacuum boundary of the domain. Also, if the wall, located at the left side, is made of dielectric material, the total current through this surface must be zero, and this boundary condition is not accomplished by the current model.

As a preliminary approach we assume constant the perpendicular current through all the streamlines in the outside region. This hypothesis and the result of $I_{i\perp}$ obtained by the PIC subcode allows us to compute $I_{e\perp}$, but then we find out that Eq. 16 for the thermalized potential leads to nonphysical results. This problem is more acute because of the low value reached by the perpendicular electron diffusivity outside the dense jet. This diffusivity follows this behavior because of the magnetic field intensity increases whereas the electron collision frequency tends to decrease. Consequently, the Hall parameter becomes higher and, according to equation 16, the required gradients of ϕ_0 to assure this electron perpendicular current are extremely high. In spite of the main problem, the charge conservation law fulfillment, according to the complete generalized Ohm law for $u_{e\perp}$, a non-isothermal model with a plasma temperature cooling outwards should contribute to a better performance of the current model. Adding anomalous turbulence would also help. These improvements will be tested in the next stage of this research. Another aspect to consider is the density parabolic profile imposed at the throat. It implies a high gradient of ϕ_0 close to the transition boundary due to the deep drop of the plasma density. Gentler profiles, such as Gaussian ones, could make easier the transition and the behavior of the thermalized potential at this transition region.

IV. Simulation results

This section presents and discuss the most interesting results so far. First, the plasma density distribution will be compared with the case in which there is not a magnetic nozzle. Then, the ion velocity vector distribution will be presented. Next, the contribution of the perpendicular electron current will be compared with ion and total currents. Afterwards, ion momentum axial contribution will be shown, in order to prove that the magnetic nozzle is an efficient device to accelerate a plasma jet. Finally, the distribution of the electromagnetic force generated by the azimuthal currents will be drawn in order to be compared with recent studies with DIMAGNO. Results have been obtained with the following parameters. Magnetic field axial intensity at the throat was 1000 Gauss. The injected ion mass flow was $\dot{m}_i = 5 \cdot 10^{-6} kg/s$. The electron temperature is 20eV. Plasma maps corresponds to results averaged over 40000 time-steps, equivalent to 0.4 milliseconds.

Figure 2 shows the plasma density distribution, for the cases with and without magnetic nozzle. The behavior is clearly different. It is also shown magnetic streamlines and ion streamlines (indeed their projection on a meridian plane). The nozzle effect is clearly illustrated and also the ion trend to detach downstream from the magnetic streamlines. In the unmagnetized case the plasma is accelerated diffusively and some ion streamlines go backwards to the left dielectric wall, where ions are recombined. Figure 3 complements the previous ones with the maps of radial and axial ion velocities. Figure 4 plots the ion azimuthal velocity, which is quite smaller than both the other two ion components and the electron azimuthal current, confirming both weak ion magnetization and thrust transmission to be dominated by the electron current.[9]

Figure 5 presents the perpendicular currents through magnetic surfaces as a function of the magnetic coordinate (λ). The perpendicular electron current is small due to strong magnetization. Again the much higher ion current indicates the low ion magnetization. The constant total electric current in the near-vacuum region is just an imposition, with no physical basis and will be revised.

Figure 6(left) shows the axial component of the ion momentum flux. It shows how an important gain is obtained compared with the reference value at the throat $F_0 = \dot{m}_i \bar{u}_i \sim 0.025N$. Finally, Fig. 6(right) shows the large azimuthal electron current at the plasma edge due to the diamagnetic drift caused by density gradients there. The electromagnetic force density $j_\theta B_r$ is the responsible of the momentum gain. The map distribution is much like the one shown by Merino and Ahedo.[11]

V. Conclusions

Hybrid code capabilities to simulate the magnetic nozzle performances and acceleration mechanisms have been analyzed. Obtained results show that the magnetic nozzle offers the advantage of guiding the plasma axially and confine it more efficiently. Our conclusions agree with the obtained results using the DIMAGNO

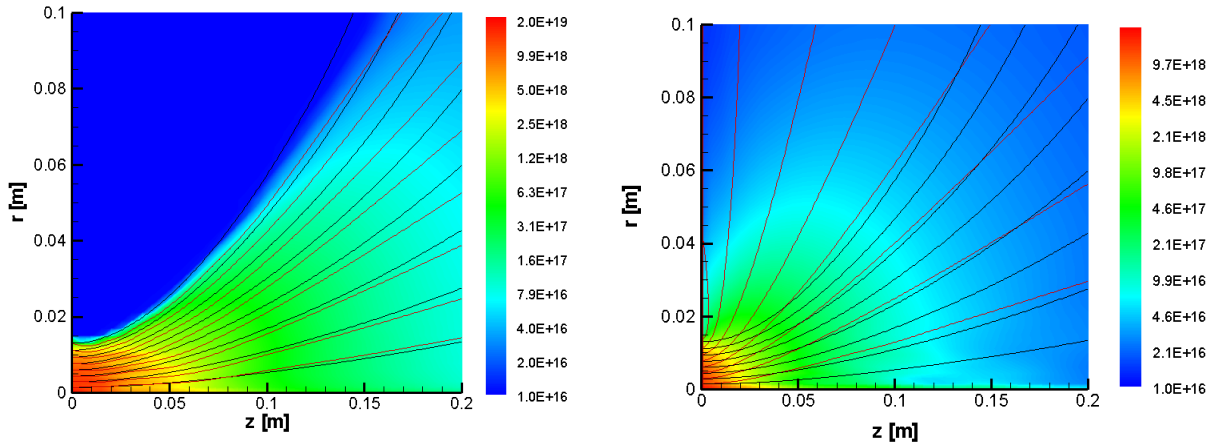

Figure 2. Plasma density distribution (in part/m^3) with magnetic nozzle effects (left) and without them (right). Magnetic streamlines are in black and ion streamlines are in red.

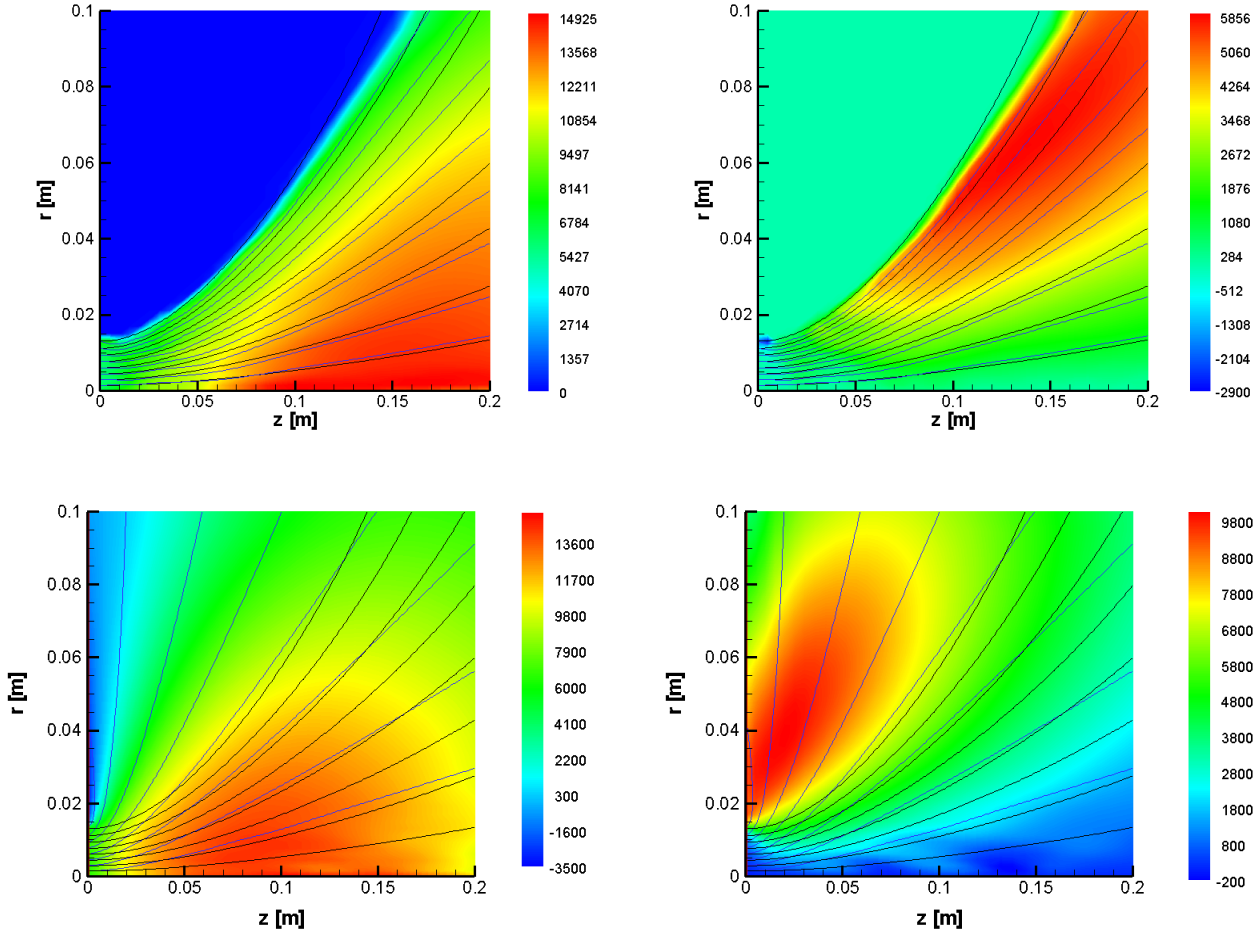

Figure 3. Ion axial (left) and radial (right) velocity (in m/s) with magnetic nozzle effects (up) and without them (down). Magnetic streamlines are in black and ion streamlines are in blue.

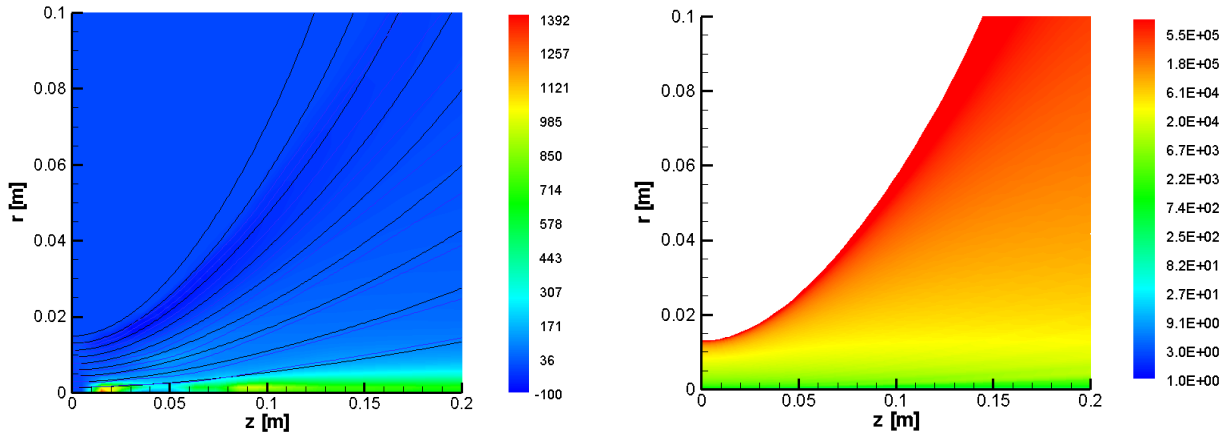

Figure 4. Ion azimuthal velocity (in m/s) with magnetic nozzle effects (left). Electron azimuthal velocity (in m/s) in the internal region (right).

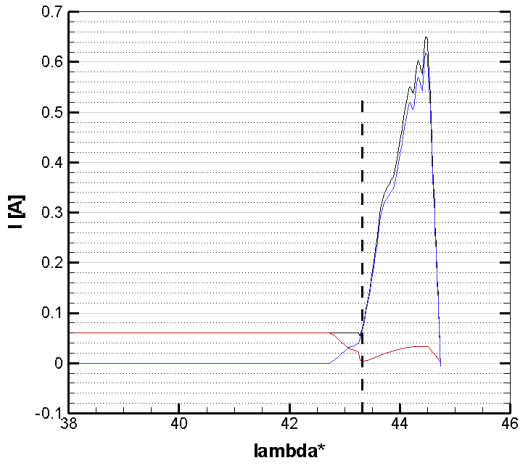

Figure 5. Perpendicular currents [A] through the magnetic surfaces as a function of the magnetic dimensionless coordinate (λ^*). Dashed vertical line separates the internal from the external region. The internal one is associated with high values of λ and it is located at the right side of the dashed line where perpendicular current is important. Outside, total current is forced to be constant. Total current is in black, ion current is in blue and electron current is in red.

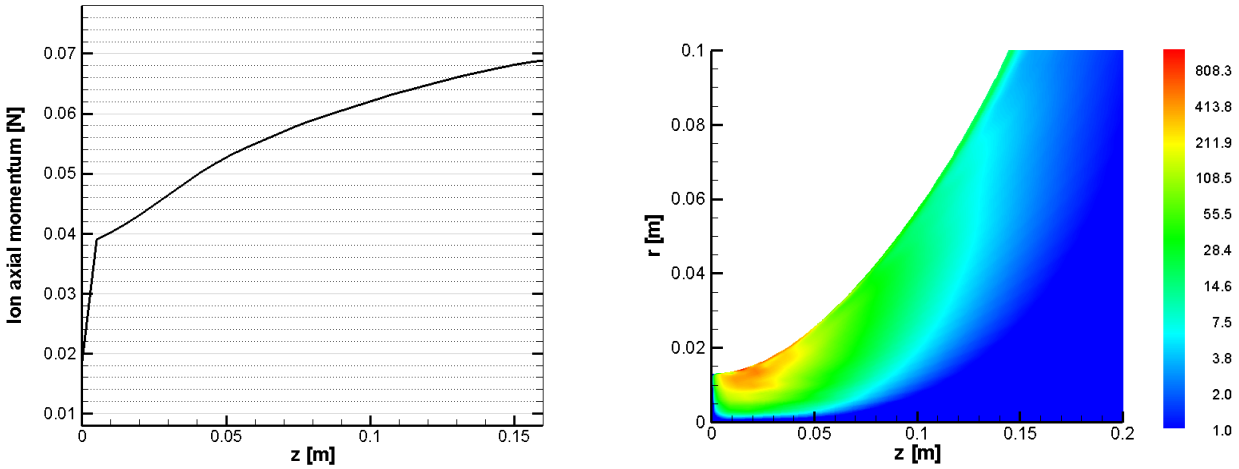

Figure 6. Ion momentum axial distribution [N] (left). Electromagnetic force per unit volume $j_\theta B_r \mathbf{1}_z [N/m^3]$ (right).

code. The comparison of plasma jets with and without magnetic effects is very illuminating too

Preliminary results indicate that the present model is more accurate in the plasma beam region, while the plasma beam edge and the near-vacuum external region, with very low plasma densities, require improvements in both PIC and electron-fluid subcodes. The following steps will be undertaken. First, the introduction of advanced algorithms on the PIC subcode for dealing with low plasma densities. Second, the development of a consistent model to assure the fulfillment of the charge conservation law and make it compatible with the existent electron diffusivity in the near-vacuum area. Third, the application of the non-isothermal model, by solving the electron energy equation.

Acknowledgments

This work was supported by the Gobierno de España under Project No. AYA2010-16699.

References

[1]Ziemba, T., Carscadden, J., Slough, J., Prager, J., and Winglee, R., "High Power Helicon Thruster," *41th Joint Propulsion Conference, Tucson, AR*, AIAA 2005-4119, American Institute of Aeronautics and Astronautics, Washington DC, 2005.

[2]Charles, C., Boswell, R., and Lieberman, M., "Xenon ion beam characterization in a helicon double layer thruster," *Applied Physics Letters*, Vol. 89, 2006, pp. 261503.

[3]Batishchev, O., "Minihelicon Plasma Thruster," *IEEE Transaction on Plasma Science*, Vol. 37, 2009, pp. 1563–1571.

[4]Pavarin, D., Ferri, F., Manente, M., Curreli, D., Guclu, Y., Melazzi, D., Rondini, D., Suman, S., Carlsson, J., Bramanti, C., Ahedo, E., Lancellotti, V., Katsonis, K., and Markelov, G., "Design of 50W Helicon Plasma Thruster," *31th International Electric Propulsion Conference, Ann Arbor, Michigan, USA*, IEPC 2009-205, Electric Rocket Propulsion Society, Fairview Park, OH, 2009.

[5]Krülle, G., Auweter-Kurtz, M., and Sasoh, A., "Technology and application aspects of applied field magnetoplasmadynamic propulsion," *J. Propulsion and Power*, Vol. 14, 1998, pp. 754–763.

[6]Arefiev, A. and Breizman, B., "Theoretical components of the VASIMR plasma propulsion concepta," *Physics of Plasmas*, Vol. 11, No. 5, 2004, pp. 2942–2949.

[7]Ahedo, E. and Merino, M., "Two-dimensional plasma acceleration in a divergent magnetic nozzle," *44th Joint Propulsion Conference, Hartford, CT*, AIAA 2009-5361, American Institute of Aeronautics and Astronautics, Washington DC, 2008.

[8]Ahedo, E. and Merino, M., "Acceleration of a focused plasma jet in a divergent magnetic nozzle," *31th International Electric Propulsion Conference, Ann Arbor, Michigan, USA*, IEPC 2009-002, Electric Rocket Propulsion Society, Fairview Park, OH, 2009.

[9]Ahedo, E. and Merino, M., "Two-dimensional supersonic plasma acceleration in a magnetic nozzle," *Physics of Plasmas*, Vol. 17, 2010, pp. 073501.

[10]Merino, M. and Ahedo, E., "Two-dimensional magnetic nozzle acceleration of a two-electron component plasma," *Proceedings of Space Propulsion 2010, San Sebastián, Spain, May 3-6, 2010*, European Space Agency, Noordwijk, The Netherlands, 2010, pp. SP2010–1841391.

[11]Merino, M. and Ahedo, E., "Simulation of plasma flows in divergent magnetic nozzles," *IEEE Transactions Plasma Science (to appear in August)*, 2011.

[12]Parra, F., Ahedo, E., Fife, M., and Martínez-Sánchez, M., "A two-dimensional hybrid model of the Hall thruster discharge," *Journal of Applied Physics*, Vol. 100, 2006, pp. 023304.

[13]Parra, F. and Ahedo, E., "Improvement of the plasma-wall interaction model on a hybrid fluid-PIC simulation of a Hall thruster," Presented at the 1st AIAA-Pegasus Student Conference, Toulouse, France.

[14]Antón, A., Escobar, D., and Ahedo, E., "Contour algorithms for a Hall thruster hybrid code," *42th Joint Propulsion Conference, Sacramento, CA*, AIAA-2006-4834, American Institute of Aeronautics and Astronautics,Washington, DC, 2006.

[15]Ahedo, E., Santos, R., and Parra, F., "Fulfilment of the kinetic Bohm criterion in a quasineutral particle-in-cell model," *Physics of Plasmas*, Vol. 17, 2010, pp. 073507.

[16]Ahedo, E. and Merino, M., "Current Ambipolarity and Plasma Detachment on a Magnetic Nozzle," *32th International Electric Propulsion Conference, Wiesbaden, Germany*, IEPC 2011-050, Electric Rocket Propulsion Society, Fairview Park, OH, 2011.